JOURNAL OF MATERIALS SCIENCE **36** (2001) 1845–1856

Microstructures and their stability in rapidly solidified Al-Fe-(V, Si) alloy powders

R. TONGSRI, E. J. MINAY, R. P. THACKRAY, R. J. DASHWOOD, H. B. McSHANE
Department of Materials, Imperial College of Science Technology and Medicine, Prince Consort Road, London SW7 2BP, UK

Microstructures and their stability in as-atomised Al-6.5Fe-1.5V and Al-6.5Fe-1.5V-1.7Si powders have been investigated using transmission electron microscopy (TEM) equipped with energy dispersive X-ray spectroscopy (EDXS), scanning electron microscopy (SEM), X-ray diffraction (XRD) and differential scanning calorimetry (DSC) techniques. It was observed that microstructures of the as-atomised powder particles showed a close relationship with powder particle sizes. The as-atomised powders exhibited three types of microstructures, namely 'zone A', 'zone B' and 'zone C'. The 'zone A' type microstructure consisted of very fine and homogeneous distributed precipitates in the α-Al matrix. The 'zone B' microstructure represented the regions consisting of microcellular structures whereas the 'zone C' microstructure represented the regions consisting of coarse cellular structures and globular quasi-crystalline phase particles. Fine powder particles exhibited both 'zone A' and 'zone B' microstructures. The size of 'zone A' decreased with increasing powder particle sizes. The intercellular phases in 'zone B' of both Al-Fe-V and Al-Fe-V-Si were very fine, randomly oriented microquasi-crystalline icosahedral particles. Microstructures of coarse powder particles exhibited both 'zone B' and 'zone C'. The intercellular phases in 'zone C' of Al-Fe-V powders could be Al_6Fe, whereas in Al-Fe-V-Si powders they were probably silicide phase. Formation of powder microstructures may be explained by the interactions between the growing α-Al fronts with the freely dispersed, primary phase particles or the solute micro-segregation. Studies using DSC techniques have revealed the microstructural stability of as-atomised powders. There were three DSC exotherms observed in the as-atomised Al-Fe-V powders. The 'zone A' was stable at elevated temperatures and the exotherm peak corresponding to the transformation reactions occurring in 'zone A' was at 360°C. The exotherm peak, which might correspond to the transformation of the globular clusters of microquasi-crystalline icosahedral phase to single-phase icosahedral particles, was at 450°C. The exotherm peak, which may correspond to the formation of $Al_{13}Fe_4$ and $Al_{45}(V, Fe)_7$ phases, was at 500°C. In the as-atomised Al-Fe-V-Si powders, only one exotherm was observed with a peak at 400°C. This exotherm may correspond to precipitation of silicide phase particles.

1. Introduction

Rapidly solidified Al-Fe based alloys are promising candidates for development of elevated temperature aluminium alloys owing to their excellent mechanical properties at both room and elevated temperatures. To achieve these properties, a microstructure consisting of homogeneously distributed thermally stable dispersoids (<100 nm diameter) is required. This can only be achieved by the application of rapid solidification technology. Several rapid solidification techniques have been developed to produce high performance materials, however, one technique, namely gas atomisation can provide sufficiently high cooling rates [1, 2] for producing desirable metastable phases or microstructures.

Since the early research on splat-cooled Al-Fe alloys [3], several rapidly solidified Al-Fe alloys have been investigated in terms of microstructural evolution [4–9] and stability [10–15]. In order to optimise the production and consolidation of this class of material, a clear understanding of the microstructural evolution during the processing is required. The thermal stability of microstructures and/or phases plays an important role in determining the mechanical properties of the as-prepared rapidly solidified materials and their products at elevated temperatures. Since rapid solidification techniques are non-equilibrium processes, the metastable phases are always associated with alloy microstructures. There are several metastable phases in rapidly solidified binary Al-Fe alloys [3–8]. Recently, the novel quasi-crystalline metastable phases, have been found in rapidly solidified aluminium alloys [16–26]. The quasi-crystalline phases observed

in rapidly solidified Al-Fe alloys have been found to be either icosahedral [27–29] or decagonal [30–33]. These phases may influence the mechanical properties of Al-Fe alloys.

Recent developments in the field of elevated temperature aluminium alloys have been focused on ternary and quaternary alloys. Rapidly solidified alloys Al-Fe-(V, Si) alloys, for example, are promising alloy systems providing excellent properties, such as strength, fracture toughness, fatigue crack growth resistance, corrosion resistance and creep rupture properties [34–41]. In this paper, the microstructures and stability of two alloy powders, namely Al-6.5Fe-1.5V and Al-6.5Fe-1.5V-1.7Si produced by gas atomisation have been investigated. This work is a part of a wider study aimed at understanding the microstructural development during processing of these alloy powders.

2. Experimental

The as-atomised Al-6.5Fe-1.5V and Al-6.5Fe-1.5V-1.7Si powders supplied by ALPOCO, were impregnated in nickel foil by an electro-chemical deposition technique [42]. The thin nickel foils, impregnated with powder particles were prepared by the electrolytic deposition of nickel. A sacrificial anode of pure nickel was employed, the cathode was made of stainless steel and highly polished to prevent the nickel from adhering. The electrolytic solution consisted of

Nickel Sulphamate ($Ni(Ni_4SO_3)_2 \cdot 4H_2O$	600 g/litre
Nickel Chloride $NiCl_2 \cdot 6H_2O$	4.4 g/litre
Boric Acid HBO_3	40 g/litre
Hydrogen Peroxide H_2O_2	2–3 drops
Distilled water	Balance

Electrolysis was conducted at a temperature of 50°C, a potential of 2.5 V, and a current density of 50 mA/cm^2. A few grams of the powder were placed onto the horizontal cathode, and were firmly incorporated within the nickel foil, which was being continuously built up during electrolysis. The whole process took around 3 hours during which time a foil of approximately 250 μm had been produced, which could be easily removed from the cathode. TEM specimens were made from the nickel foil by jet electropolishing using 10 volume percent of perchloric acid in ethanol at 65 V and −45°C. Microstructures and phase identifications were carried out using a Phillips PW 1700 series XRD machine, a JEOL FX2000 Mk 1 TEM, and EDS analysis. Scanning electron microscopy was performed using a JEOL JSM 220 machine. The thermal stability of powder microstructures was investigated by using a Stanton Redcroft 1500 DSC machine, scanned at the temperature range of 25–600°C at a scan rate of 10°C/min. The volume median diameter (D[v,0.5]) of each powder size fraction was obtained by using a Malvern Laser Particle Sizer.

3. Results and discussion

3.1. General microstructures

Microstructures of the as-atomised Al-Fe-V and Al-Fe-V-Si powders with diameters up to 65 μm were found to exhibit similar microstructural morphologies (when both alloy powder particles with the same diameters were compared). The variations in structural morphology with powder particle size, resulting from different cooling rates, undercoolings and solidification velocities, could be observed. The transition of microstructural morphologies within an individual powder particle was also observed. Details of powder microstructures are given below.

TEM observations revealed that microstructures of fine powder particles with diameters of up to 5 μm consisted of two regions (Fig. 1a and b). The first region designated as 'zone A' exhibited fine precipitates distributed homogeneously in the α-Al matrix as shown on the left-hand side of Fig. 1c. The second region designated as 'zone B' exhibited typical microcellular structures as shown on the right-hand side of Fig. 1c. Note that the designation 'zone A' used in this article is slightly different from that of the original 'zone A' designated by Jones [3] for conventional optically featureless microstructures. The 'zone A' in the article of Jones can be compared to both designations 'zone A' and 'zone B' as used in this paper.

In powder particles with medium sizes (with diameters of 5–15 μm), two groups of powder particles exhibiting different microstructures were observed. The first group of powders exhibited microstructures consisting of 'zone A' and 'zone B' (Fig. 2a). The size of 'zone A' decreased with increasing powder particle sizes and completely disappeared in a powder particle larger than 10 μm. The second group of powder particles exhibited almost entirely 'zone B' (Fig. 2b). The cell spacings were observed to increase with increasing distance away from the nucleation site, which was usually at the droplet surface. In some powder particles, globular primary phase particles were observed in the regions consisting of coarse cellular microstructures. The microstructures consisting of coarse cells or dendrites with globular primary phase particles were designated as 'zone C'. The globular primary phase particles were reported to form independently in the melt by homogeneous nucleation and diffusionless growth with rates of 1–2 m/s in melt-spun Al-Fe alloys [27].

In powder particles with coarse sizes (with diameters bigger than 15 μm), microstructures were observed to consist of 'zone B' and 'zone C'. The sizes of cell spacing in 'zone C' increased with increasing distance away from the nucleation site and with increasing powder particle size (Fig. 3a). The diameters of globular primary phase particles also increased gradually with increasing distance away from the boundary between 'zone B' and 'zone C' and with increasing powder particle size. The transition boundary of growth from the microcellular (zone B) to the coarse cellular or dendritic (zone C) modes could be observed using SEM (Fig. 3b).

3.2. Microstructural development

Formation of 'zone A' or a similar microstructure is complicated and not well understood. Chu and Granger [8] have suggested that the formation of fine

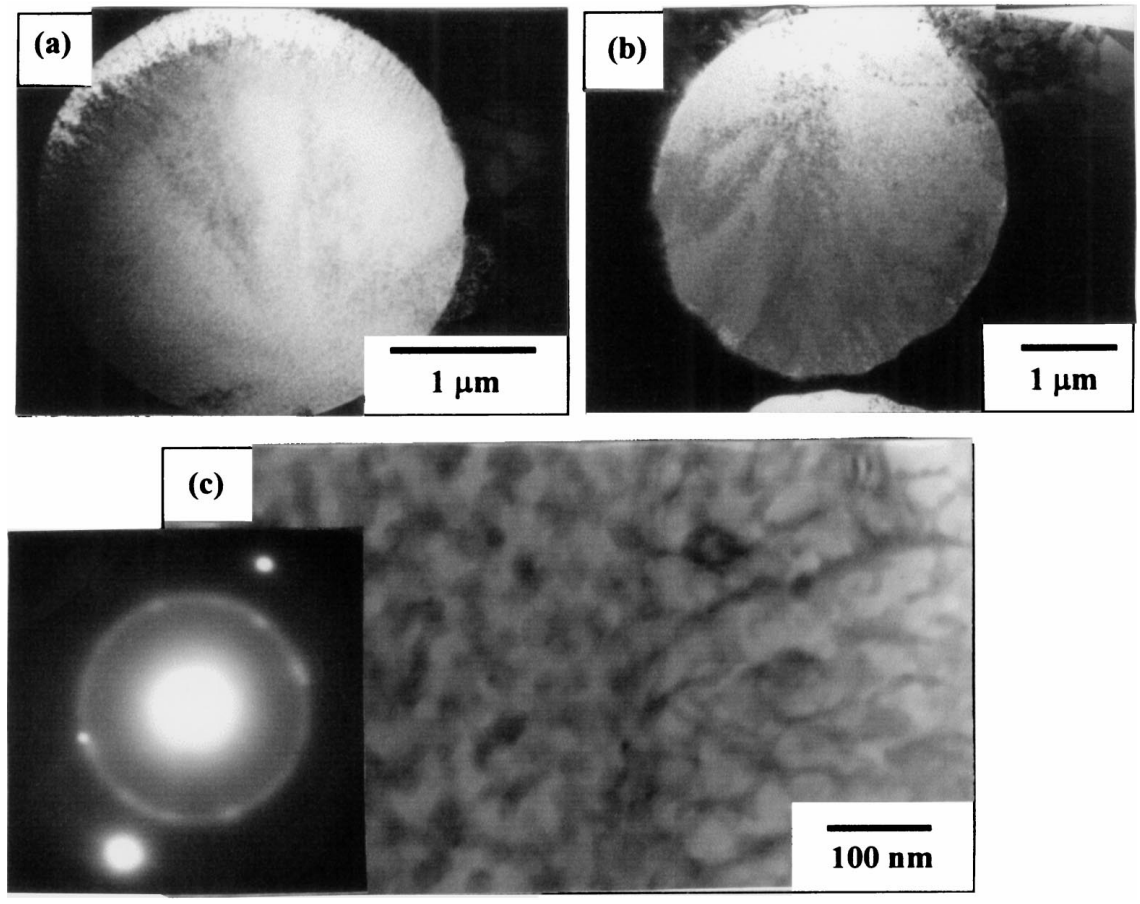

Figure 1 Bright field TEM images showing; (a) a fine Al-Fe-V powder particle, (b) a fine Al-Fe-V-Si powder particle, and (c) 'zone A' and 'zone B' microstructures in fine Al-Fe-V-Si powder particles.

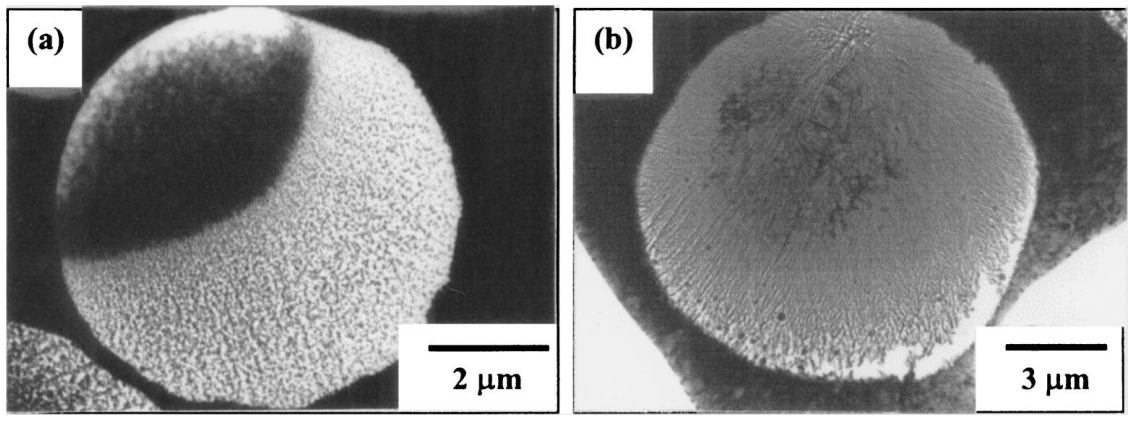

Figure 2 Bright field TEM images of medium Al-Fe-V powder particles; (a) a powder particle exhibiting 'zone A' and 'zone B' microstructures, (b) a powder particle exhibiting 'zone B' and 'zone C' microstructures.

precipitates in 'zone A' of melt-spun binary Al-Fe alloys was attributed to the segregation during solidification rather than solid-state decomposition after solidification because of their random orientation with respect to the α-Al matrix. Boettinger *et al.* [7] have found that the morphological transition of the intercellular phases occurred according to the solidification velocity in a rapidly solidified Al-Fe-Ni alloy. They have reported that the intercellular phase morphology changed from continuous forms at medium velocities (indicated by electron beam scan velocities of between 2.5 cm/s–100 cm/s) to discrete rounded particles at high velocities (indicated by electron beam scan velocities $>$ 100 cm/s). A mechanism for the occurrence of round particles at high velocities involves the formation and subsequent solidification of the isolated droplets of solute-rich liquid within the α-Al matrix. The droplets are formed by a pinching-off of liquid in the grooves in a cellular liquid/solid interface.

Selected area electron diffraction pattern (SADP) of 'zone A' of Al-Fe-V and Al-Fe-V-Si powders exhibited a ring pattern similar to the SADP of microcellular structures ('zone B' see Fig. 4b), except that the number of rings in the former pattern was less than that in the latter one. This may indicate that fine precipitates in 'zone A' form during solidification so they

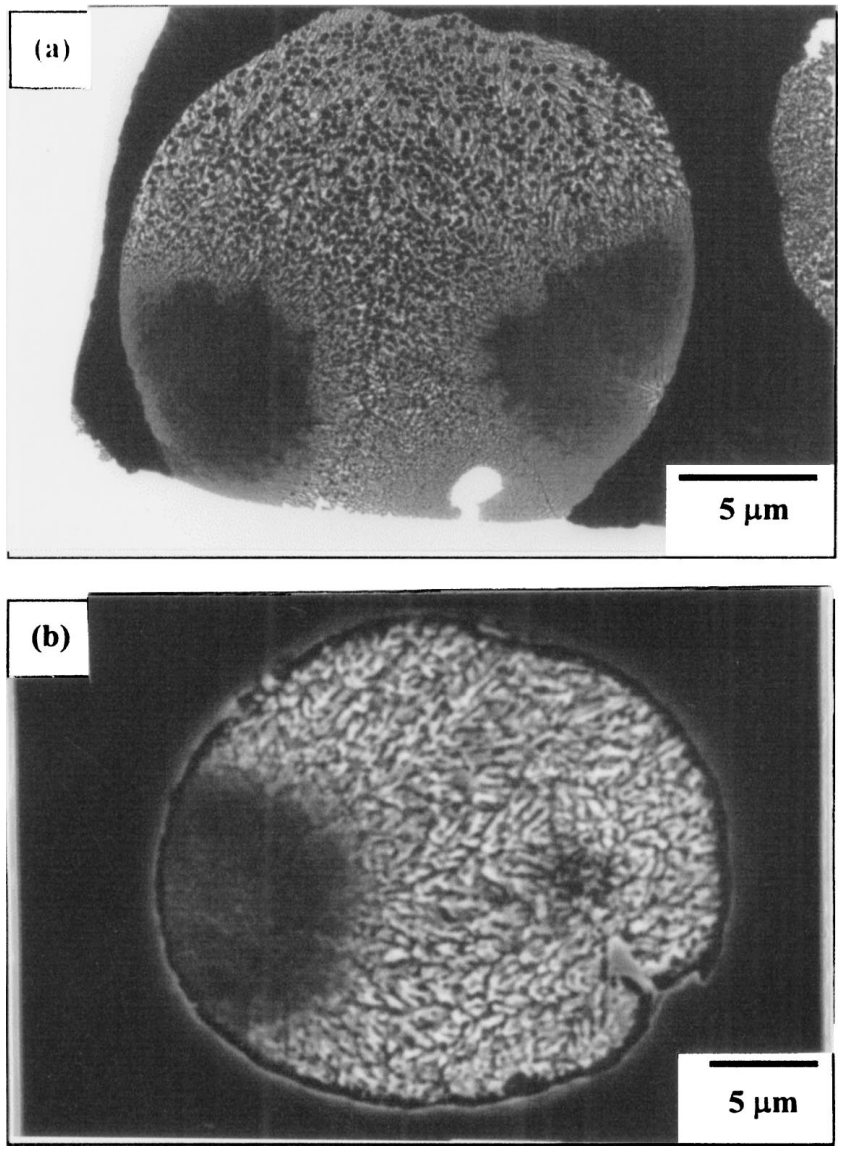

Figure 3 Microstructures of coarse Al-Fe-V powder particles; (a) bright field TEM image, and (b) SEM image. The figure shows the microstructural transition from 'zone B' to 'zone C' microstructures.

are randomly oriented with respect to the α-Al matrix after solidification. A similar SADP was reported to result from the icosahedral phase in 'zone A' of melt-spun Al-V-Fe [43] and Al-Fe-V-Si [39] alloys. By using the convergent beam electron diffraction (CBED) technique, fine precipitates in 'zone A' microstructures of a melt-spun Al-Fe-Mo-V ribbon [24] were found to be microquasi-crystalline icosahedral (MI) particles. It may be possible that fine precipitates in 'zone A' of fine Al-Fe-V and Al-Fe-V-Si powder particles could be MI particles distributed uniformly and oriented randomly with respect to the α-Al matrix.

The microstructural development during solidification of powder particles may be explained using two assumptions. The first may be explained by using the interactions between solidification fronts and freely suspended particles [44–46]. During solidification, freely suspended small particles may be either pushed or engulfed by a solidification front depending on the size of the particles and the velocity of the solidification front. Higher solidification front velocities are required to engulf finer particles rather than coarse ones.

According to the first assumption, the formation of 'zone A' may be explained as follows. In an undercooled alloy melt droplet, nucleation events of the MI phase may occur throughout a droplet. The MI particles grow and suspend freely in the alloy liquid. While the MI particles are growing, the α-Al phase nucleates and then grows with a planar front at extremely high velocities. The freely suspended MI particles are engulfed in the α-Al matrix as a result of the interaction between the solidifying front and the particles. A similar explanation may also be given for the formation of 'zone B' and 'zone C'. The formation of 'zone B' may be explained as follows. When α-Al grows with a cellular front at high velocities, MI particles may be pushed laterally and entrapped in the intercellular regions. The limited volume of alloy melt in the intercellular regions may limit the further growth of the MI particles. For 'zone C', when α-Al grows with a coarse cellular or dendritic front at decreased velocities, the MI particles may allowed to grow further before the interactions occur. The growth of the MI phase may result in the formation of coarse globular primary phase particles. Note

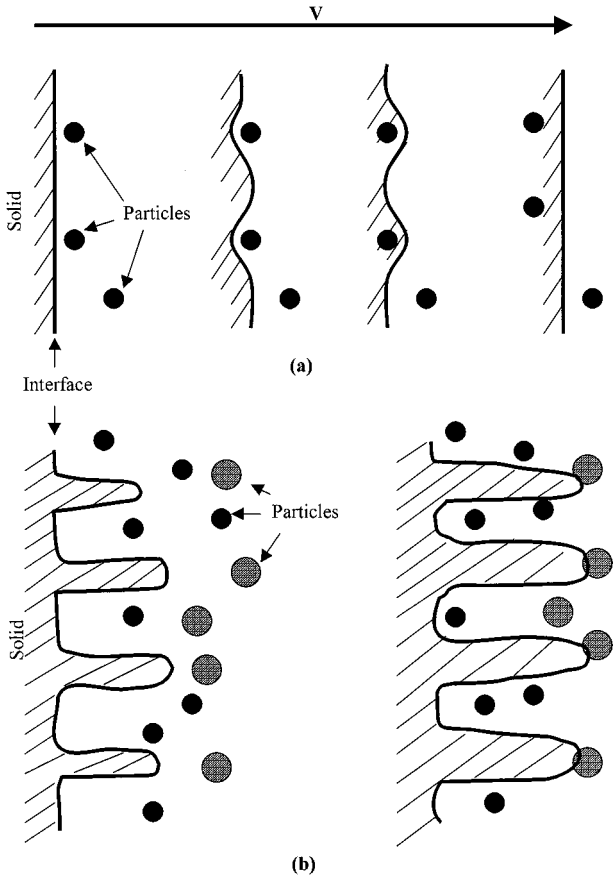

Figure 4 Schematic diagram showing interaction between second phase particles and planar (a) and cellular (b) solidification fronts (adapted from Asthama *et al.* [44]).

that in Al-Fe-V powders most coarse globular primary phase particles were speculated to be globular clusters of MI (GCMI) particles whereas in Al-Fe-V-Si powders some were GCMI and some were globular single-phase icosahedral (I) particles (Section 3.3.2). The GCMI or I particles may be pushed by the solidification front for some distance before being trapped at intercellular/interdendritic regions. A schematic diagram showing the interactions between the solidifying fronts and the freely suspended particles is shown in Fig. 4. Evidence of particle engulfment (left hand side of Fig. 1c), particle entrapment in the intercellular regions (right hand side of Fig. 1c), and particle pushing (Fig. 3a) seem to support this assumption.

The second assumption for evolution of powder microstructures may be explained by using the solute micro-segregation during solidification. When an alloy melt droplet is undercooled to a certain temperature below the melting point, nucleation of α-A1 occurs first. While the α-A1 front grows, it rejects the solutes into the liquid ahead of the front. Formation of intermetallic phases then occurs in the solute-rich liquid. For the formation of 'zone A' and 'zone B', the α-A1 front may grow with a cellular front at high velocities resulting in formation of fine cells. The solutes may be rejected to the liquid ahead of the growing front and the intercellular regions. Because the cellular front grows at high velocities into the liquid, more content of solutes may be rejected laterally into the intercellular regions where the intermetallic phases form. For the formation of 'zone C', the α-A1 front may grow with a cellular front at decreased velocities resulting in the formation of coarse cells. In the solute-rich liquid ahead of the slow growing cell front, some globular particles may nucleate and grow until the cells trap them. In the solute-rich intercellular liquid, some intermetallic phases may also form.

3.3. Phase identifications in the as-atomized Al-Fe-V powders

3.3.1. Phase identifications by XRD

Table I contains the summary of the observed *d*-values and the relative intensities of the phases present in Al-Fe-V powders (excluding those of aluminium peaks). Relative intensities in the table are quoted in relative values to the Al (111) peak. Phase identifications were carried out by comparing the observed *d*-values and intensities of the unknown phases with those of the known phases given in the JCPDS diffraction data cards, i.e. number 41-1285 for Al_6Fe phase, and number 44-1195 for quasi-crystalline (QC) phases, respectively. Unlike indexing of diffraction patterns of normal crystals, sets of six digit numbers may be used to index diffraction patterns of the QC phases [19, 20]. The indices of the XRD peaks from the QC phases in Table I were obtained by following the description given by Bancel *et al*. [16], and Audier and Guyot [23].

It was apparent that two phases were detected in Al-Fe-V powder particles, namely Al_6Fe and QC phases. The XRD peaks corresponding to the Al_6Fe phase could be detected in all powder fractions. The Al_6Fe is the common phase found in several rapidly solidified Al-Fe based alloys. Formation of this phase in binary Al-Fe

TABLE I XRD data and possible phases in Al-Fe-V powder particles

	Powder volume median diameter, (D[v,0.5], μm)						
Observed *d*-spacing (nm)	8	11	14	23	37	50	Possible phase
0.384	0.3	0.5	0.3	0.6	0.4	0.4	QC (110 001)
0.243	2.1	1.8	1.5	1.4	1.9	1.6	unknown
0.217	0.8	1.8	2.0	3.0	3.1	3.8	QC (100 000) + Al_6Fe
0211	0.2	2.9	2.2	2.0	1.8	0.6	Al_6Fe
0.206	3.0	3.2	4.5	5.2	5.9	6.4	QC (110 000) + Al_6Fe
0.150	0.2	0.3	0.4	0.6	0.4	0.3	QC (111 000) + Al_6Fe
0.127	0.3	0.4	0.4	0.7	0.9	0.9	QC (101 000) + Al_6Fe
	Relative Intensity (I/I_0)						

alloys requires cooling rates greater than 5 K/s [5] and growth rates greater than 0.1 mm/s [4]. The calculated cooling rates associated with the production of aluminium and aluminium alloy powders with diameters of up to 100 μm by gas atomisation were reported to be in the range of 10^2–10^5 K/s [1, 2]. This range of cooling rates is sufficient for the formation of Al_6Fe in Al-Fe-V powders. Some XRD peaks (with observed *d*-values of 0.217 nm and 0.206 nm) of Al_6Fe were observed to overlap with those of the QC phases.

The icosahedral edge length, *a*, calculated from the XRD data by using the method outlined by Audier and Guyot [23] was found to be 0.5101 ± 0.0037 nm. The value *a* in rapidly solidified binary Al-Fe and Al-V alloys was observed to be independent of composition over a wide composition range; *a* is about 0.508 nm and 0.526 nm in Al-Fe and Al-V, respectively [38]. However, the value *a* in rapidly solidified ternary Al-Fe-V alloys was reported to be dependent on the Fe : V atomic ratio [15, 38] for example in the alloys with composition of $Al_{87}(V, Fe)_{13}$, the value of *a* decreased (from the value *a* of Al-V to the value *a* of Al-Fe) with increasing Fe content or Fe : V atomic ratio. Because the Al-Fe-V powders investigated in this study have a nominal composition of Al-6.5Fe-1.5V and thus have the Fe : V atomic ratio of about 4 : 1, the value *a* in these alloy powders can be expected to be close to that of binary Al-Fe alloys. The value *a* of the I-phases in Al-Fe-V powders obtained in this investigation suggests that such an expectation is true.

3.3.2. Phase identifications by TEM and EDS

The bright field TEM image and the electron diffraction pattern of globular particles in Al-Fe-V powders are shown in Fig. 5a. The pattern consists of several electron diffraction rings. The measured *d*-values and relative intensities of electron diffraction rings (Table II) were compared to those of the I-Al_4Mn phase [23] and it was found that they matched very well. It was also noticed that the diffuse rings with observed *d*-values of 0.217 and 0.206 nm exhibited strong intensities. Moreover, the observed *d*-values of globular particles in Al-Fe-V powders obtained from the electron diffraction pattern (Table II) were found to match with the observed *d*-values obtained by XRD techniques given in Table I. The EDS analyses performed on several globular particles revealed that their composition was Al_x(Fe, V) where *x* was in the range of 5 to 6.

In fact the single-phase icosahedral particles exhibit electron diffraction patterns which display sharp spots with fivefold, threefold, and twofold rotationally symmetric axes. An example of such electron diffraction pattern of the icosahedral phase particle in Al-Fe-V-Si powders is shown in Section 3.4.2. However, only ring patterns could be obtained from the globular particles in coarse Al-Fe-V powder particles. This may be attributed to the fact that the globular particles are clusters of microquasi-crystalline icosahedral (GCMI) particles. The globular phase is therefore designated here as GCMI- Al_x(Fe, V).

The electron diffraction pattern of microcellular structures or zone B microstructures of Al-Fe-V powders (Fig. 5b) was observed to be similar to that of the GCMI-Al_x(Fe, V) phase mentioned above. The observed *d*-values of the diffracted rings from 'zone B' microstructures were close to those of the GCMI-Al_x(Fe, V) phase. In addition to the strong diffracted rings with observed *d*-values of 0.217 and 0.206 nm, a rather diffuse band expanding from the observed *d*-value of 0.145 nm to the observed *d*-value of 0.117 nm was also observed in the electron diffraction pattern of 'zone B' microstructures. The electron diffraction patterns with ring characters may indicate that the intercellular phases in the 'zone B' microstructures could be very fine and randomly oriented microquasi-crystalline icosahedral (MI) phase particles.

The MI phases have also been observed in the microcellular structures (similar to zone B of RS-Al-Fe-V powders) of laser surface treated Al-Fe [28, 29] and melt-spun Al-Fe-Si alloys [47]. The other form of quasi-crystalline phases, designated as T′ phase, has also been found in microcellular structures of melt-spun Al-Fe-Mo and Al-Fe-Ce alloys [22, 24]. The T′ phases were in fact decagonal (D) phases [17].

In this study, no attempt has been made to identify the D phase in the intercellular regions. However, it is speculated that the D phase may solidify in conjunction with the MI phase in intercellular liquid of zone B. The formation of the D phase is favoured at slower solidification velocities or slower quenching rates than those

TABLE II Showing the measured *d*-values, relative intensities and indexing of an I-A1$_x$(Fe, V) phase particle and the intercellular phase in Al-Fe-V powders, compared to the values of the I-Al_4Mn phase [23]

	GCMI-Al_x(Fe, V) particle		Intercellular phase		I-Al_4Mn		
Ring number[Z]	Observed *d*-value (nm)	I/I_0[H]	Observed *d*-value (nm)	I/I_0[H]	Reported *d*-value (nm)	I/I_0	Indexing
R1	0.382	M + D	0.382	M + D	0.3850	22	110001
R2	0.217	S + D	0.217	S + D	0.2170	100	100000
R3	0.206	S + D	0.206	S + D	0.2065	78	110000
R4	0.145	W	0.145-		0.1459	11	111100
R5	0.126	W	0.117	W + D	0.1275	20	101000
R6	0.108	W	0.108	W	0.1085	7	200000

Note: ([Z]) See Fig. 5.
([H]) W = weak, M = medium, S = strong, and D = diffused.

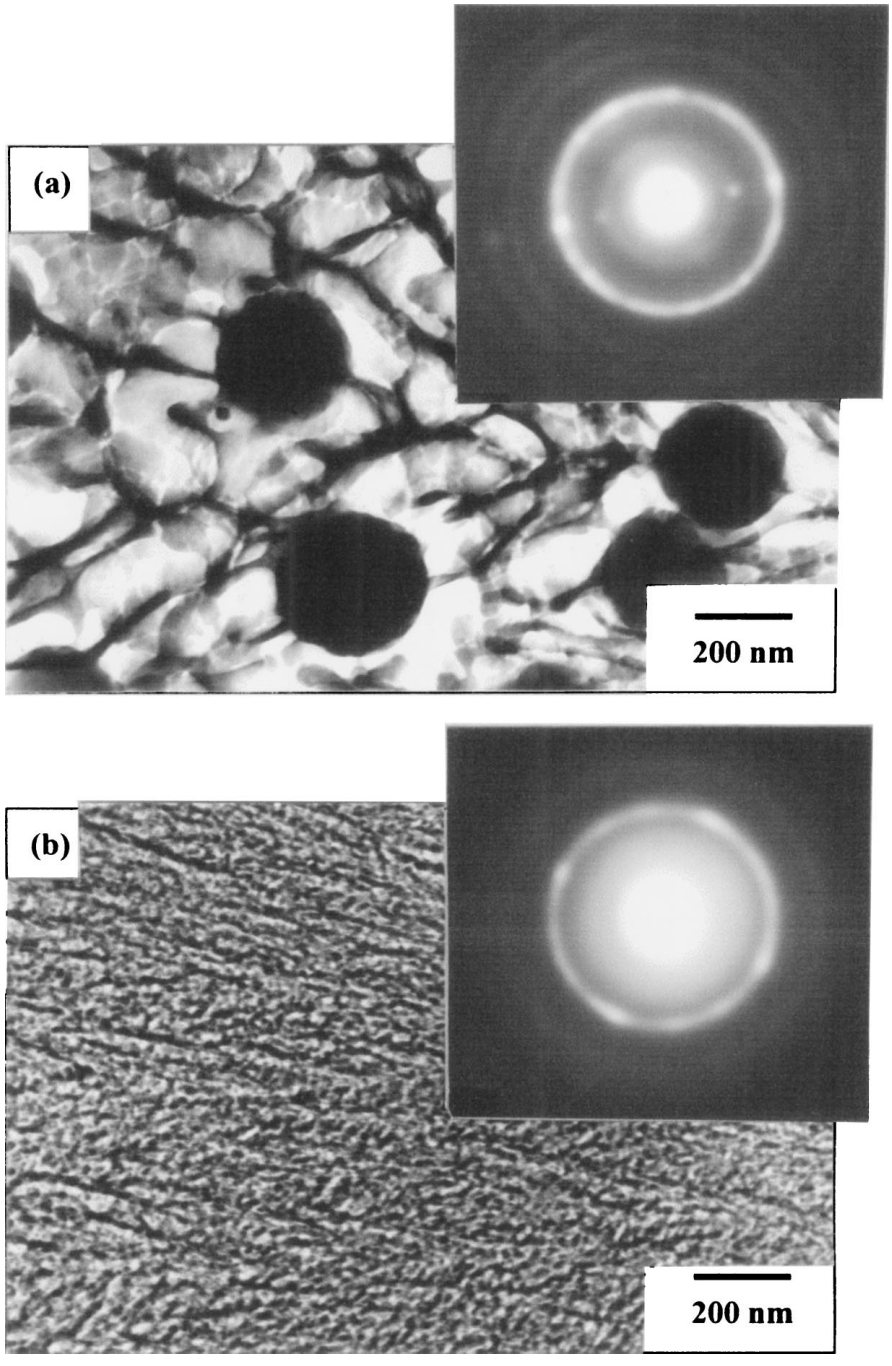

Figure 5 Bright field TEM images and electron diffraction patterns of; (a) GCMI-Al_x(Fe, V) phase particles, and (b) intercellular phase particles.

required for the formation of the icosahedral phase [18, 21, 25, 26]. The solute rich intercellular liquid in 'zone B', resulting from solute rejection during solidification of cellular α-Al front, contains freely dispersed MI particles. During the solidification of the α-Al phase, the temperature of the intercellular liquid is expected to increase due to latent heat released by recalescence. The increased temperature is not high enough to dissolve the MI particles, but is able to reduce the level of undercooling. Thus solidification velocities of the intercellular liquid are slow. Both high solute content and increased temperature can probably promote the formation of D phase on the surface of MI phase. The D phase has been observed to solidify on the surface of I phase in rapidly solidified Al-Mn alloys when the solidification velocities decreased [18, 21].

The EDXS analyses performed on coarser cellular structures with cell spacings of 180–360 nm in 'zone C' microstructures revealed the segregation of the iron and vanadium elements (Fig. 6). It was observed that although there was supersaturation of iron within the cells, this element tended to segregate to cell walls or intercellular regions where the formation of Al_6Fe phase might occur. Only small amounts of vanadium could be detected both within cells and at cell walls. Depletion of this element in the cell interiors and cell walls of coarse cellular structures in 'zone C' microstructures may be attributed to the fact that vanadium was consumed by the growth of the GCMI-Al_x(Fe, V) phase particles during solidification.

In the as-atomised Al-Fe powders, the Al_6Fe phase has been observed to exist in the form of rod-shaped

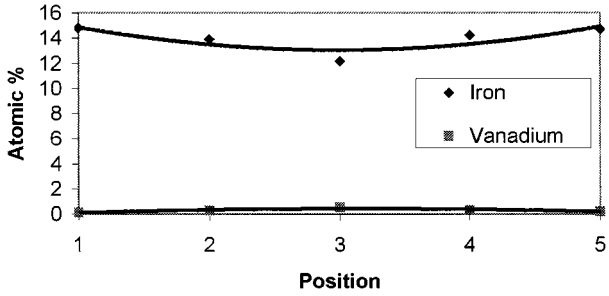

Figure 6 Plot of solute contents as functions of positions determined across coarse cellular structures (zone C) of coarse RS-Al-Fe-V powder particles: position 1 = cell wall, position 2 = near cell wall, position 3 = cell center, position 4 = near cell wall, and position 5 = cell wall, respectively.

Al-Al_6Fe eutectics in the intercellular/interdendritic regions [6]. However, the Al-Al_6Fe eutectics were not observed in the as-atomised-Al-Fe-V powders. The absence of the eutectic structure may be attributed to the higher solidification velocities. Recently, in laser surface treated Al-4 at. % Fe, the transition from Al-Al_6Fe eutectic to primary Al-dendrites was observed to occur at high solidification rates (≥ 0.9 cm/s) [9].

A similar morphological transition with solidification velocity has also been observed in a rapidly solidified Al-Fe-Ni alloy [7]. A eutectic α-Al-Al_9(Fe, Ni)$_2$ microstructure changed to a continuous Al_9(Fe, Ni)$_2$ microstructure in the intercellular regions when the solidification velocities changed from low (indicated by electron beam scan velocities less than 2.5 cm/s) to medium velocities (indicated by electron beam scan velocities of between 2.5 cm/s–100 cm/s).

3.4. Phase identifications in the as-atomised Al-Fe-V-Si powders

3.4.1. Phase Identifications by XRD

The XRD data for Al-Fe-V-Si powders are shown in Table III (excluding those of α-Al). By using the JCPDS numbers 6-669 and 44-1195, the XRD peaks could be identified as the reflections from silicide and QC phases.

When the lattice parameter of the bcc-Al_{13} (Fe, V)$_3$Si phase, with a value of 1.2607 nm [35], and set of integers, $s = (h^2 + k^2 + l^2) = 2, 4, 6, 8, 10$, etc. for a bcc crystal structure system, were employed for calculation of the d-values, it was found that the calculated d-values matched quite well with the experimental values shown in Table III. The XRD data indicate that there are two phases, namely I-phase and bcc-Al_{13} (Fe, V)$_3$Si phase, existing in Al-Fe-V-Si powders.

The quasi-lattice parameter, a, for Al-Fe-V-Si powders was calculated using XRD data and found to be 0.5102 ± 0.0013 nm. The values of quasi-lattice parameters for both Al-Fe-V and Al-Fe-Ve-Si powders were the same. This indicates that addition of silicon to the ternary Al-Fe-V alloys has a minimal effect on the value of a. This result is consistent with the previous study on the nature of the I-phases in melt-spun Al-(Fe, V, Si) alloys [38].

3.4.2. Phase Identifications by TEM and EDS

Electron diffraction patterns of some globular particles in 'zone C' microstructures of Al-Fe-V-Si powders (Fig. 7) exhibited sharp spots like those obtained from a single crystal. The diffraction spot array did not posses a long-range periodically translational order, but showed crystallographically forbidden rotational symmetry of fivefold rotation axis. In addition to the fivefold symmetry, electron diffraction patterns of the globular particles also exhibited other aperiodically rotational symmetries, namely threefold, twofold, and pseudo twofold symmetries. It was found that the composition of the globular particles determined by EDS was (Al, Si)$_x$(Fe, V) where x was in the range of 5 to 6. The particles exhibiting SADPs with diffraction spots are designated as 'I-(Al, Si)$_x$(Fe, V)'. It was also found that not all of the globular particles exhibited diffraction spots. Some of them exhibited electron diffraction patterns with ring characters similar to those of the GCMI-Al_x(Fe, V) phase. The particles exhibiting SADPs with diffraction rings are designated as 'GCMI-(Al, Si)$_x$(Fe, V)'.

Identification of the intercellular phases in 'zone B' microstructures of Al-Fe-V-Si powders using selected area electron diffraction techniques (Fig. 8) revealed that the observed d-values (Table IV) corresponding to electron diffraction rings were close to those of intercellular phases in 'zone B' microstructures of Al-Fe-V powders. It may be concluded that the intercellular phases in 'zone B' microstructures of

TABLE III XRD data and possible phases in RS-Al-Fe-V-Si powders

Observed d-spacing (nm)	Powder volume median diameter, (D[v,0.5], μm)				Calculated d-spacing of silicide (nm)	Possible phase
	7	11	17	31		
0.445	0.2	0.2	0.3	0.4	0.446	Silicide
0.400	0.5	0.7	1.7	1.3	0.400	Silicide
0.343	02	0.2	0.4	0.2	0.364	Silicide
0.337	0.2	0.2	0.2	0.3	0.337	Silicide
0.258	0.2	0.4	0.2	0.2	0.257	Silicide
0.247	0.4	0.3	1.1	0.6	0.247	Silicide
0.217	1.7	2.3	4.0	2.9	0.216	Silicide + QC
0.210	0.5	0.7	0.7	1.7	0.210	Silicide + QC
0.149	0.2	0.3	0.3	0.2	0.149	Silicide
0.127	1.2	1.4	1.8	1.1	0.127	Silicide + QC
	Relative intensity (I/I_0)					

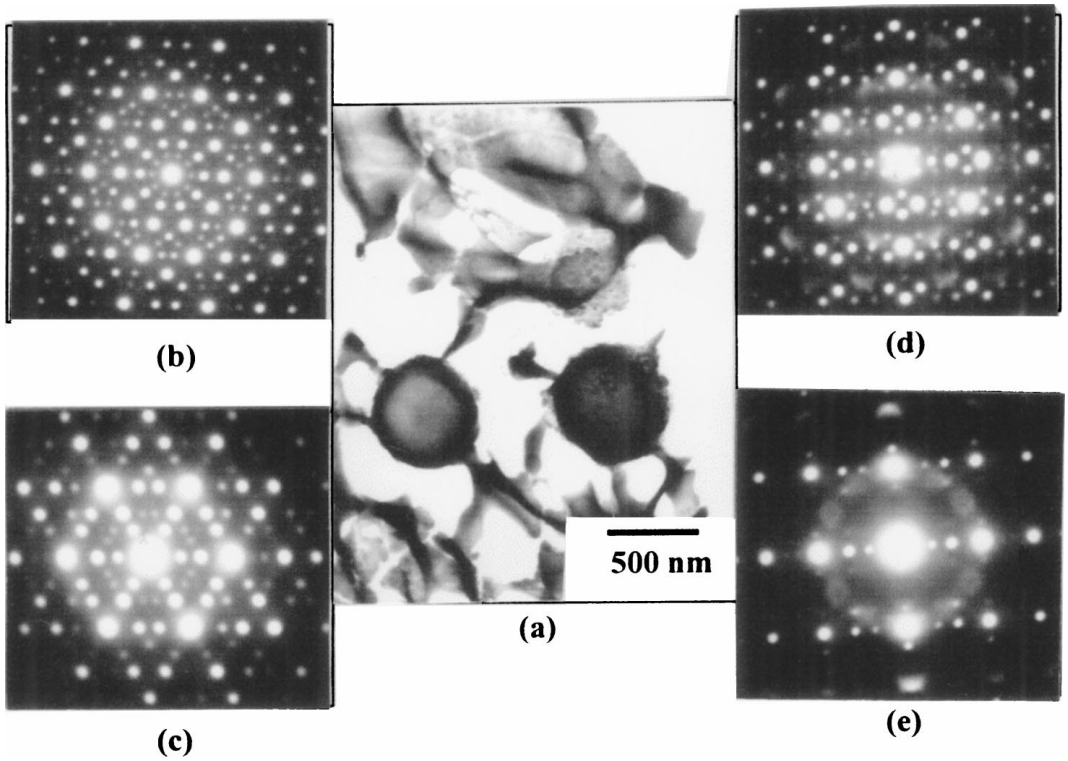

Figure 7 Bright field TEM image of I-$(Al, Si)_x$(Fe, V) particles in 'zone C' microstructures of Al-Fe-V-Si powders (a) and electron diffraction patterns showing fivefold (b), threefold (c), twofold (d), and pseudo twofold (e) symmetries, respectively.

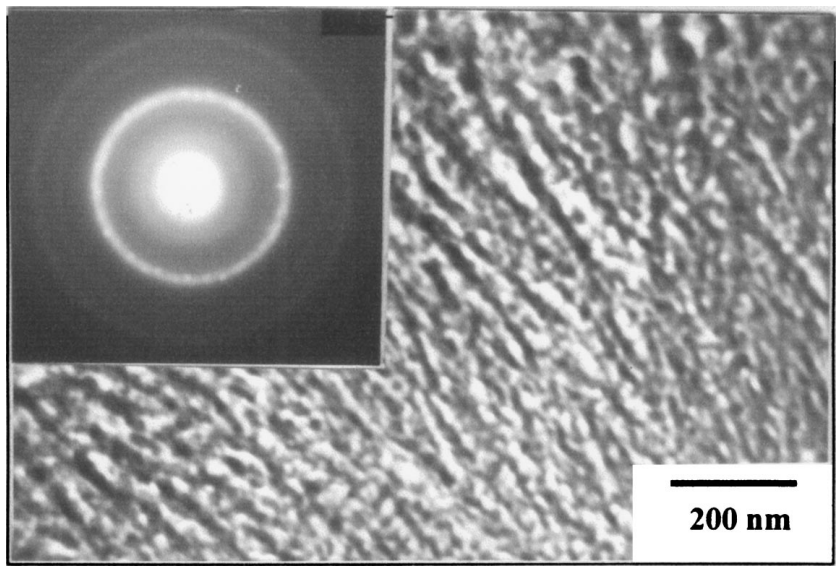

Figure 8 'Zone B' microstructures and electron diffraction pattern of Al-Fe-V-Si powders.

Al-Fe-V-Si powders could be very fine and randomly oriented MI particles. This result is consistent with the previous phase identifications in melt-spun Al-Fe-V-Si alloys [39, 40].

The microstructures of coarse cells in 'zone C' microstructures of Al-Fe-V-Si powders exhibited precipitation within cells (Fig. 9). Chemical analysis by EDS across the cells (Fig. 10) revealed that there was no significant segregation of silicon and vanadium across the cells. There was a slightly higher amount of iron segregated to cell walls compared to that segregated to the cell interiors. The insignificant segregation across the coarse cells may support the evidence of the existence of precipitates within cells. The cell walls themselves could also be the same phase (silicide) as the precipitates within the cells.

3.5. Microstructural stability of the as-atomised powders

Microstructural stability of the as-atomised powders was investigated by employing DSC scanning in the temperature range of 25 to 600°C and with a heating rate of 10°C/min. The DSC curves of the as-atomised powders (Fig. 11) show the exotherms, which correspond to phase transformation reactions occurring during heating of the alloy powders. Since the DSC exotherms were broad and the onset temperatures were difficult to

TABLE IV Comparison of the observed *d*-values and intensities of electron diffraction patterns from the intercellular phases in the 'zone B' microstructures of Al-Fe-V and Al-Fe-V-Si powders

	Al-Fe-V Powders		Al-Fe-V-Si Powders	
Ring Number	*d*-value (nm)	Int.	*d*-value (nm)	Int.
R1	0.382	M + D	0.382	W + D
R2	0.217	S + D	0.215	S + D
R3	0.206	S + D	0.206	S + D
R4			0.147	W
R5	0.145-0.017	W + D	0.126	M
R6	0.108	W	0.108	W

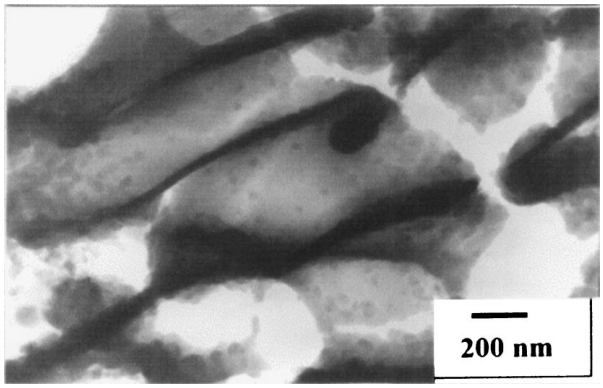

Figure 9 Coarse cells in 'zone C' microstructures of Al-Fe-V-Si powders.

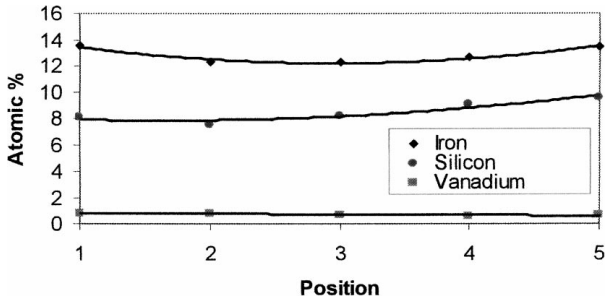

Figure 10 Plot of solute contents as functions of positions determined across coarse cellular structures (zone C) of coarse RS-Al-Fe-V-Si powder particles: positions 1–5 are defined the same as those in Fig. 6.

determine, the peak temperatures were chosen to represent the exotherms. The DSC curves of the as-atomised Al-Fe-V powders were observed to vary with powder size or diameter and they were also different from those of the as-atomised Al-Fe-V-Si powders. Details concerning the microstructural stability of these two alloy powders are given below.

3.5.1. The as-atomised Al-Fe-V powders

Three exotherms, designated as exotherm A, exotherm B, and exotherm C representing the exotherms with peak temperatures of about 360, 500 and 450°C, respectively, were observed in the as-atomised Al-Fe-V powders (Fig. 11).

The exotherm A was observed only in fine powder particles. This may indicate that the exotherm A relates to transformation reactions occurring in 'zone A' microstructures. It was speculated that the MI phase could

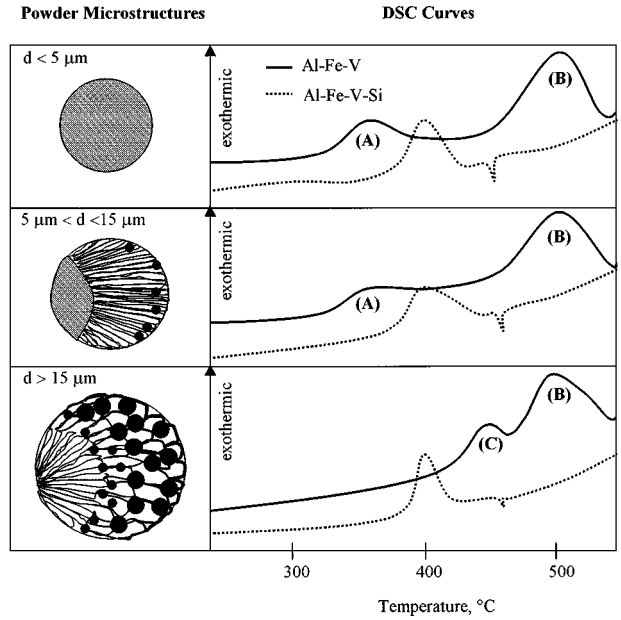

Figure 11 Schematic diagram showing microstructures and DSC curves of Al-Fe-V and Al-Fe-V-Si powder particles.

be present in both 'zone A' and 'zone B' microstructures, but the exotherm A disappeared in the coarser powder particles, which contained 'zone B' microstructures. This may suggest that the transformation reaction of the MI phase could not correspond to the exotherm A. The possible phase transformation corresponding to the exotherm A could be the decomposition of the supersaturated solid solution in 'zone A' microstructures.

The exotherm B was observed in all powder particle sizes. To examine the nature of the reaction corresponding to this exotherm, fine Al-Fe-V powder particles were heat-treated at 500°C for up to 30 minutes and the phases in the heat-treated powder particles were characterised using TEM and XRD. Microstructures (Fig. 12) of heat-treated powder particles clearly exhibited needle-like particles of $Al_{13}Fe_4$ and $Al_{45}(V, Fe)_7$. The XRD data (Table V) also confirmed the existence of $Al_{13}Fe_4$ and $Al_{45}(V, Fe)_7$. Microstructures of the as-extruded alloys produced from Al-Fe-V powders also exhibited needle-like particles of $Al_{13}Fe_4$ and $Al_{45}(V, Fe)_7$ [48]. The possible reaction corresponding to exotherm B may be attributed to precipitation of $Al_{13}Fe_4$ and $Al_{45}(V, Fe)_7$.

The reaction corresponding to exotherm B has been a controversial subject of interpretation. The exotherms, obtained from differential thermal analysis (DTA), with peak temperature of 444°C for rapidly solidified

TABLE V Observed *d*-values, relative intensities and possible phases in heat-treated Al-Fe-V powder particles

Observed *d*-value (nm)	Relative intensity	Possible phase [48]
0.394	1.2	$Al_{13}Fe_4$
0.350	0.7	$Al_{13}Fe_4$
0.333	0.6	$Al_{13}Fe_4$
0.215	1.8	$Al_{13}Fe_4 + Al_{45}(V, Fe)_7$
0.209	4.0	$Al_{13}Fe_4 + Al_{45}(V, Fe)_7$
0.206	4.3	$Al_{13}Fe_4 + Al_{45}(V, Fe)_7$

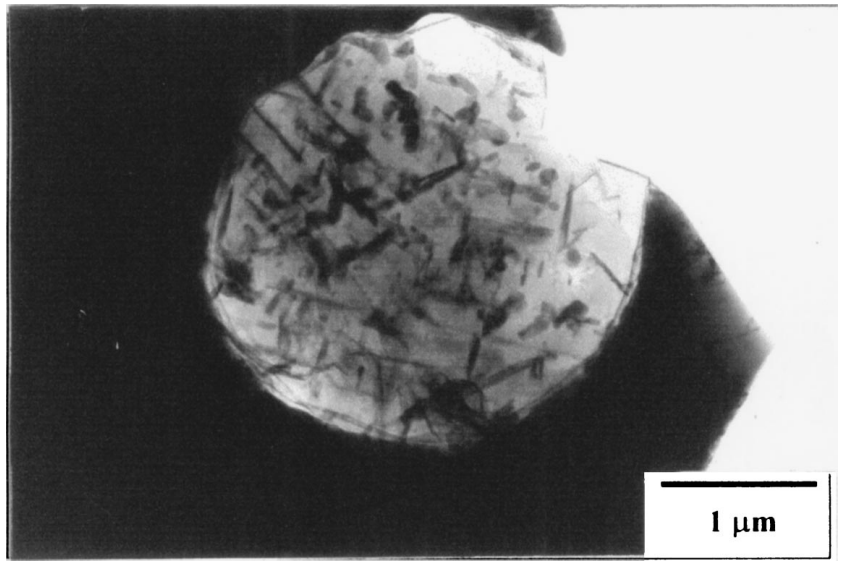

Figure 12 Microstructures of an Al-Fe-V powder particle treated at 500 °C for 15 min.

Al-8 wt. % Fe and of 495°C for rapidly solidified Al-10 wt. % Fe-2 wt. % V, have been claimed to be attributed to precipitation of $\theta'Al_3Fe$ [10]. The precipitation of equilibrium $\theta'Al_3Fe$ was claimed to occur at about 595°C in Al-8 wt. % Fe. However, DTA studies of melt-spun $Al_{86}Fe_{14}$, have shown that the reaction corresponding to the exotherm around 527–577°C was the transition from Al_6Fe to Al_3Fe [12]. The DSC exotherm corresponding to the same reaction was found to be about 450°C in melt-spun Al-8 wt. % Fe [12].

The exotherm C was observed in coarse powder particles. The magnitude of this exotherm increased with increasing powder particle size. This trend was consistent to the increase of size and volume fraction of the GCMI-Al_x(Fe, V) particles with increasing powder particle size.

3.5.2. The as-atomised Al-Fe-V-Si powders

There was only one exotherm with a peak temperature at 400°C observed on the DSC curves of Al-Fe-V-Si powder particles (Fig. 11). One exotherm may indicate that several phase transformation reactions occur at nearly the same temperature. However, it was mentioned in Section 3.4 that there were phases, i.e., silicide, I-(Al, Si)$_x$(Fe, V), and GCMI-(Al, Si)$_x$(Fe, V), observed in Al-Fe-V-Si powder particles. Since the silicide phase was found to be very stable due to slow coarsening rates (2.9×10^{-26} to 8.4×10^{-27} m^3/h at 425°C) [35, 37, 38] the transformation of this phase at 400°C (exotherm peak temperature) could be ruled out. The possible phase transformation reaction corresponding to the DSC exotherm may be the decomposition of the I-(Al, Si)$_x$(Fe, V) and GCMI-(A1, Si)$_x$(Fe, V) particles. The decomposition temperature at which the globular particles transformed to the bcc α-Al_{12}(Fe, V)$_3$Si particles was found to be 400°C for a melt-spun Al-Fe-V-Si alloy [39]. This temperature (400°C) is consistent with the exotherm peak temperature obtained in this investigation.

4. Conclusions

There is similarity in the microstructural morphologies of the as-atomised Al-Fe-V and Al-Fe-V-Si powders, although the phases present in these two alloy powders are slightly different. The microstructural morphologies designated as 'zone A', 'zone B' and 'zone C', can be observed in both alloy powder particles. 'Zone A' represents the microstructures consisting of very fine precipitates. 'Zone B' represents the microstructures consisting of microcells. 'Zone C' represents the microstructures consisting of coarse cells and/or dendrites with globular particles. 'Zone A' and 'zone B' are typical microstructures of fine to medium powder particles whereas 'zone C' is usually observed in coarse powder particles.

In the as-atomised Al-Fe-V powder particles, 'zone A' microstructures are stable at elevated temperatures up to 360°C. This is indicated by the peak temperature of the exotherm A. The possible phase transformation reactions occurring in 'zone A' may be the decomposition of supersaturated solid solution. 'Zone B' microstructures are stable up to 500°C. This is indicated by the peak temperature of the exotherm B. The reactions corresponding to this exotherm could be the precipitation of $Al_{13}Fe_4$ and Al_{45}(V, Fe)$_7$. The GCMI-Al_x(Fe, V) phase is believed to transform to single-phase I phase at 450°C. This reaction corresponds to the exotherm C.

In contrast, there is only one exotherm peak observed in the as-atomised Al-Fe-V-Si powder particles. This exotherm may correspond to the precipitation of the silicide phase particles from metastable globular phases occurring at 400°C.

Since all phase transformation reactions occur at temperatures $\leq$ 500°C, it can be expected that during the powder consolidation at such temperatures the microstructures of the as-atomised powder particles will transform to the intermetallic phases mentioned above. The powder consolidation at temperatures higher than 500°C may result in coarsening of the phases. The

coarsening of phases is not desirable for processing of alloys.

Acknowledgements

One of the authors, R. Tongsri, would like to thank the Royal Thai Government, the European Commission (BRITE EURAM), and technical support at the Department of Materials, Imperial College.

References

1. N. J. GRANT, *J. Metals* **35** (1983) 20.
2. W. WANG, D. LIU and N. J. GRANT, *Scripta Metall.* **21** (1987) 1279.
3. H. JONES, *Mater. Sci. Eng.* **5**(1) (1969/70) 1.
4. I. R HUGHES and H. JONES, *J. Mater. Sci.* **11** (1976) 1781.
5. R. M. K. YOUNG and T. W. CLYNE, *Scripta Metall.* **15** (1981) 1211.
6. W. J. BOETTINGER, L. BENDERSKY and J. G. EARLY, *Metall. Trans. A.* **17A** (1986)781.
7. W. J. BOETTINGER, L. A. BENDERSKY, R. J. SCHAEFER and F. S. BIANCANIELLO, *ibid.* **19A** (1988) 1101.
8. M. G. CHU and D. A. GRANGER, *ibid.* **21A** (1990) 205.
9. P. GILGIEN, A. ZRYD and W. KURZ, *Acta Metall. Mater.* **43**(9) (1995) 3477.
10. I. J. POLMEAR, M. J. COUPER and M. J. BANNISTER, *Mater. Forum.* **12** (1988) 54.
11. R. A. DUNLAP and K. DINI, *Can. J. Phys.* **63** (1985) 1267.
12. R. M. K. YOUNG and J. H. TWEED, *Mater. Sci. Eng.* **A134** (1991) 1153.
13. J. L. MURRAY, A. J. MCALLISTER, R. J. SCHAEFER, L. A. BENDERSKY, F. S. BIANCANIELLO and D. L. MOFFAT, *Metall. Trans. A.* **18A** (1985) 385.
14. D. J. SKINNER, V. R. V. RAMANAN, M. S. ZEDALIS and N. J. KIM, *Mater. Sci. Eng.* **99** (1988) 407.
15. M. S. ZEDALIS, V. R. V. RAMANAN and D. J. SKINNER, in "Thermal Analysis in Metallurgy," edited by R. D. Shull and A. Joshi (The Mineral, Metals & Materials Society, Pennsylvania, 1992) p. 279.
16. P. A. BANCEL, P. A. HEINEY, P. W. STEPHENS, A. I. GOLDMAN and P. M. HORN, *Phys. Rev. Lett.* **54**(22) (1985) 2422.
17. L. BENDERSKY, *ibid.* **55**(14) (1985) 1461.
18. L. BENDERSKY, R. J. SCHAEFER, F. S. BIANCANIELLO, W. J. BOETTINGER, M. J. KAUFMAN and D. SHECHTMAN, *Scripta Metall.* **19** (1985) 909.
19. J. W. CAHN, D. SHECHTMAN and D. GRATIAS, *J. Mater. Res.* **1**(1) (1985) 13.
20. V. ELSER, *Phys. Rev. B.* **32**(8) (1985) 4892.
21. R. J. SCHAEFER and L. BENDERSKY, *Scripta Metall.* **20** (1985) 745.
22. J. W. ZINDEL, P. KURATH and H. L. FRASER, in "High Strength Powder Metallurgy Aluminum Alloys II," edited by G. J. Hildeman and M. J. Koczak (The Metallurgical Society, Pennsylvania, 1985) p. 213.
23. M. AUDIER and P. GUYOT, *Phil. Mag. B.* **53**(1) (1986) L43.
24. R. D. FIELD, J. W. ZINDEL and H. L. FRASER, *Scripta Metall.* **20** (1986) 415.
25. F. GILLESSEN and D. M. HERLACH, *Mater. Sci. Eng.* **A134** (1991) 1220.
26. K. F. KELTON, *Int. Mater. Rev.* **38**(3) (1993) 105.
27. C. M. ADAM, V. R. V. RAMANAN and D. J. SKINNER, in "Undercooled Alloy Phases," edited by E. W. Collings and C. C. Koch (The Metallurgical Society, Pennsylvania, 1987) p. 59.
28. M. GREMAUD, M. CARRARD and W. KURZ, *Acta Metall. Mater.* **38**(12) (1990) 2587.
29. M. CARRARD, M. GREMAUD and M. PIERANTONI, *Scripta Metall. Mater.* **25** (1991) 925.
30. K. K. FUNG, C. Y. YANG, Y. Q. ZHOU, J. G. ZHAO, W. S. ZHAN and B. G. SHEN, *Phys. Rev. Lett.* **56**(19) (1986) 2060.
31. X. D. ZOU, K. K. FUNG and K. H. KUO, *Phys. Rev. B.* **35**(9) (1987) 4526.
32. K. H. KUO, *Mater. Sci. Forum.* **22–24** (1987) 131.
33. D. H. KIM and B. CANTOR, *Phil. Mag. A.* **69**(1) (1994) 45.
34. P. S. GILMAN and S. K. DAS, in Proceedings of International Conference on PM Aerospace Materials (A Metal Powder Report Conference) Luzern, November 2–4, 1987 (MPR Publishing Services, Shrewsbury 1988) Vol. 27.1.
35. D. J. SKINNER, in "Dispersion Strengthened Aluminum Alloys," edited by Y.-W. Kim and W. M. Griffith (The Minerals, Metals and Materials Society, 1988) p. 181.
36. M. A. RODRIGUEZ and D. J. SKINNER, *J. Mater. Sci. Lett.* **9** (1990) 1292.
37. N. J. KIM, *Int. J. Rapid Solidification* **6** (1991) 175.
38. V. R. V. RAMANAN, D. J. SKINNER and M. S. ZEDALIS, *Mater. Sci. Eng.* **A134** (1991) 912.
39. W. J. PARK, S. AHN and N. J. KIM, *ibid.* **A189** (1994) 291.
40. Y. L. TANG, S. K. GUAN, D. S. SHAO, N. F. SHEN and H. Q. HU, *J. Mater. Sci. Lett.* **12** (1993) 1749.
41. P. GILMAN, *Metals and Materials* **6** (1990) 504.
42. R. J. DASHWOOD, Ph.D. thesis, University of London, 1990.
43. E. S. HUMPHREYS, P. J. WARREN and A. CEREZO, *Mater. Sci. Eng.* **A250** (1998) 158.
44. R. ASTHANA, P. K. ROHATGI and S. N. TEWARI, in "Microstructure Formation during Solidification of Metal Matrix Composites," editing by P. K. Rohatgi (The Minerals, Metal & Materials Society, TMS, Warrendale, PA, 1993) p. 11.
45. D. SHANGGUAN, S. AHUJA and D. M. STEFANESCU, *Metall. Trans. A.* **23A** (1992) 669.
46. (a) F. R. JURETZKO, B. K. DHINDAW, D. M. STEFANESCU, S. SEN and P. A. CURRERI, *Metall. Mater. Trans. A.* **29A** (1998) 1691; (b) D. M. STEFANESCU, F. R. JURETZKO, B. K. DHINDAW, A. CATALINA, S. SEN and P. A. CURRERI, *ibid.* **29A** (1998) 1697.
47. L. A. BENDERSKY, A. J. MCALISTER and F. S. BIANCANIELLO, *ibid.* **19A** (1988) 2893.
48. TONGSRI R, Ph.D thesis, University of London 2000.

Received 4 August
and accepted 5 September 2000